

Design, Dynamic Modeling, and Experimental Validation of A Novel Alternating Flow Variable Displacement Hydraulic Pump

Mengtang Li^{ID}, Ryan Foss, Kim A. Stelson, James D. Van de ven^{ID}, and Eric J. Barth^{ID}

Abstract—High power density, good controllability, and low cost are the most appealing characteristics that make hydraulic systems the best choice for many applications. Current state-of-the-art hydraulic variable displacement pumps show high efficiency at high displacement while they have poor efficiencies at low displacement. This paper proposes a novel alternating flow (AF) variable displacement hydraulic pump to: 1) eliminate metering losses by acting as a high-bandwidth pump for displacement control; 2) achieve high efficiency across a wide range of operating conditions and displacements; and 3) allow multiple units to be easily common-shaft mounted for a compact multi-actuator displacement control system from a single prime mover. A dynamic model using first principles describes the cylinder pressure, flows between pairs of cylinders, and net inlet and outlet flows as a function of the pumps phase-shift angle. The model captures hydraulic check valve dynamics, the effective bulk modulus, leakage flows, and viscous friction. Piston kinematics and dynamics are discussed and energy loss models are presented. A first prototype of the AF pump was constructed from two inline triplex pumps that were modified so that three piston pairs were created. Experiment tests were conducted and used to validate the model. After model validation, simulation results from the model can offer an initial evaluation of this novel pump concept and potential applications and can be used to guide the design for future prototype of the AF hydraulic pump.

Index Terms—Alternating flow (AF) hydraulics, modeling and validation, variable displacement pump.

I. INTRODUCTION

TADITIONAL hydraulic circuits use metering valves to control the load, resulting in precise control and fast response. However, metering valve control results in significant

Manuscript received February 6, 2018; revised August 3, 2018; accepted March 17, 2019. Date of publication March 21, 2019; date of current version June 14, 2019. Recommended by Technical Editor Prof. H. Moon. This work was supported by the Center for Compact and Efficient Fluid Power (CCEFP) under NSF Grant 0540834 with funding from the National Fluid Power Association (NFPA) Education and Technology Foundation. (*Corresponding author: Eric John Barth.*)

M. Li and E. J. Barth are with the Department of Mechanical Engineering, Vanderbilt University, Nashville, TN 37235 USA (e-mail: mengtang.li@vanderbilt.edu; eric.j.barth@vanderbilt.edu).

R. Foss, K. A. Stelson, and J. D. Van de Ven are with the Department of Mechanical Engineering, University of Minnesota, Minneapolis, MN 55455 USA (e-mail: fossx231@umn.edu; kstelson@umn.edu; van.deven@umn.edu).

Color versions of one or more of the figures in this paper are available online at <http://ieeexplore.ieee.org>.

Digital Object Identifier 10.1109/TMECH.2019.2906859

energy dissipation, which is largely the reason that the average efficiency of a hydraulic system is as low as 21% [1]. Load sensing (LS) circuits are widely used in the industry to control the pressure source to match with the highest pressure load to minimize the throttling loss. An LS system does improve the system efficiency but when the required pressure levels from different loads are not close to each other, LS still suffers from throttling loss and poor efficiency. Instead of throttling the fluid and transforming the unnecessary power into heat, a more efficient alternative is to drive each actuator with a variable displacement pump and control the actuator with the pump displacement, termed displacement control [2]. An excavator employing displacement control with currently available variable pump/motors has experimentally demonstrated 39% energy savings over throttling valve control in a load sensing circuit [3]. The modularity of displacement control brings another benefit. It makes the whole system more reliable than a single pump circuit with throttling valves. If one pump fails, the other axes are decoupled and still fully functional. Critical to displacement control is the performance and efficiency of the variable displacement pump across a wide range of displacements and pressures. For multiactuator circuits, where multiple pumps are driven on a common shaft, the package size and weight of the pump are also important.

The family of variable positive displacement pumps includes vane pump, axial piston pump, bent axis pump, radial piston pump, along with some new architectures. Although much work has been done on improving the maximum efficiency of these variable displacement pumps [4]–[7], such pumps characteristically have low efficiency at low volumetric displacement since the largest energy losses do not scale with output power [8]. Axial piston pumps accommodate a through shaft, but are axially long making it challenging to common-shaft mount multiple pumps. Bent axis pumps are a variation of the axial piston machine with low piston side-loading, offering higher efficiencies. However, these pumps are typically more expensive and more complex and do not offer through shaft configurations. Vane pumps can also be variable, but incur high side loads on the pump shaft, operate at lower pressure levels, and have lower efficiency. Radial piston pumps are axially short and accommodate a through shaft, making them package well. They are also highly efficient and operate at higher pressures. However, currently, only few variable configurations are available beyond the Moog RKP, which also suffers from high shaft loads. Two

1083-4435 © 2019 IEEE. Personal use is permitted, but republication/redistribution requires IEEE permission.
 See http://www.ieee.org/publications_standards/publications/rights/index.html for more information.

relatively new architectures include the Artemis Digital Displacement pump and the variable displacement linkage pump. The Artemis pump offers very high efficiencies and packages well due to its radial piston configuration. This pump, however, relies on the precise timing of inlet and outlet valves for fluid management. The variable displacement linkage pump uses a changing ground pivot of six-bar linkage to decrease swept volume while maintaining a constant dead/unswept volume. This pump offers very high efficiencies across a wide operating range but is bulky in the inline configuration and complex in the radial configuration [9].

An alternative to a mechanically variable displacement pump is to vary the flow rate of a fixed displacement pump through the speed control of an electric drive motor, known as electro-hydraulic actuator (EHA). While straightforward and more efficient, the high cost and lower power density of electronics restricts the usage of EHA [10]. The flow rate could also be controlled with high-speed switching of digital valves, termed digital displacement. The most common approach to digital displacement is flow diverting, where the actively controlled tank valve is held open for a portion of the upstroke of the piston, returning the fluid to tank. At a specified displacement fraction of the piston stroke, the tank valve is rapidly closed and the pressure valve is opened, sending flow to the load. While this approach eliminates the leakage and friction of the port plates of an axial piston or bent axis pump, it has several drawbacks. The valve transitions occur at high piston velocity, resulting in throttling energy loss across the partially open tank and pressure valves for a fraction of the piston stroke and generating water hammer creating noise and large flow pulsations [11], [12]. Viscous flow losses are incurred by pumping the unused flow back to tank, and there is a lack of digital valves with reasonable energy consumption that can switch fast enough for high-speed pumps.

Alternating flow hydraulics (AFH) is a special class of hydraulics characterized by the transmission of power with no net flow. Over the last century, work pertaining to AFH has been intermittent, beginning with Constantinescos published work back in the early 1900s [13]. Weng developed a hybrid AFH-DC flow system called a pulsating flow system for the use of two different fluids [14]. Davis applied a lumped parameter transmission line method, commonly used in electrical systems, to AF hydraulic transmission [15]. And more recently, Marcu developed a prototype rotary hydraulic motor that is powered by alternating flow [16]. Although the geometry presented in the AF pump is too small for the effects of travelling pressure waves to be relevant, it nonetheless inspired the concept.

This paper proposes a novel AF hydraulic pump with the aim of eliminating throttling energy loss, having high efficiency across a wide range of operating conditions and displacements, and being compact to allow multiple units to be easily common-shaft mounted. In Section I, the basic principles of the AF hydraulic pump are presented. Next, dynamic models describing the cylinder pressure and flow rate between the connecting pipes are discussed in detail in Section II. The model also captures hydraulic check valve dynamics and the effective bulk modulus. Section III describes an input motor torque model and various

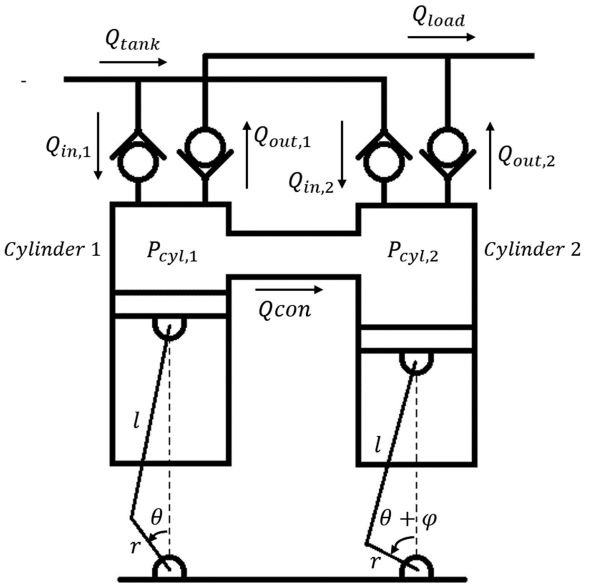


Fig. 1. AF hydraulic pump concept.

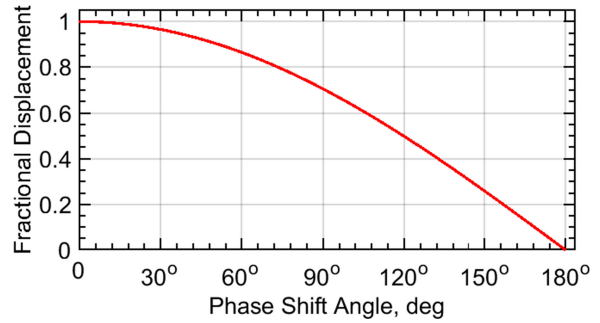


Fig. 2. Variable displacement as a function of the phase-shift angle.

energy loss models. The construction of AF pump prototype 1 along with experiment tests are presented in Section IV. Simulation results from the model are compared with experiment tests in Section V and a discussion follows in Section VI. Section VII provides the concluding remarks.

II. AF PUMP

The proposed AF hydraulic pump is formed by joining two radial piston pumps. Each pumping pair can be viewed as two sinusoidally oscillating pistons of equal displacement with cylinders directly connected by a fluid conduit, as shown in Fig. 1. The output flow rate reaches a maximum when the motions of the two pistons are in phase. When the motions of the two pistons are 180 degrees out of phase, fluid is shuttled back and forth, resulting in zero net output flow rate. Continuously variable displacement is achieved through the variation of the phase-shift angles between the pistons, as shown in Fig. 2.

The architecture of the radial piston pump provides the AF hydraulic pump with several inherent benefits. First, it is one of the most efficient pump architectures of the current state of the art. Second, it has a short axial compact size and can have a

through shaft, which allows multiple units to be common-shaft mounted to control a multiple actuator system. Third, with a multilobe cam, an AF hydraulic pump can achieve extremely high displacement density. The shift angle required for varying displacement is also reduced.

III. AF PUMP DYNAMIC MODEL

A lumped parameter model is developed for each pair of pumping piston cylinders. A set of differential equations need to be solved numerically to obtain cylinder pressure $P_{\text{cyl},i}$ in i th piston cylinder

$$\dot{P}_{\text{cyl},i} = \frac{\beta_{\text{eff}}}{V_{\text{cyl},i}} (Q_{\text{in},i} - Q_{\text{out},i} - Q_{\text{leak},i} - Q_{\text{con}} - \dot{V}_{\text{cyl},i}) \quad (1)$$

where β_{eff} is the pressure-dependent effective bulk modulus, the inlet flow rate $Q_{\text{in},i}$ is defined positive if oil flows into the cylinder, the output flow rate $Q_{\text{out},i}$ is defined positive if oil flows out of the cylinder, leakage flow $Q_{\text{leak},i}$ is assumed to be unrecoverable, and the flow rate through the connecting pipe Q_{con} is defined positive if oil flows from cylinder 1 to cylinder 2.

A simple kinematic model is used in this paper to describe the motion of each piston. The positions of piston 1 and piston 2 from the same pair are given by

$$y_1 = r(1 - \cos \theta) + l - \sqrt{l^2 - r^2 \sin^2 \theta} \quad (2)$$

$$y_2 = r(1 - \cos(\theta + \phi)) + l - \sqrt{l^2 - r^2 \sin^2(\theta + \phi)} \quad (3)$$

where θ is the rotated angle and ϕ is the phase-shift angle.

Rotation of the first piston is assumed to start from its top dead center. Then, the instantaneous volume for one pair of piston cylinders is

$$V = 2V_{\text{tdc}} + V_{\text{con}} + A_p(y_1 + y_2) \quad (4)$$

where V_{tdc} is the unswept dead volume of each cylinder chamber, V_{con} is the volume of the connecting pipe, and A_p is the surface area of each piston.

For the sake of simplicity, (4) can be approximated as follows if the connecting rod length l is at least three times longer than the crank radius r :

$$V = 2V_{\text{tdc}} + V_{\text{con}} + \frac{\pi d_p^2 r}{2} \left[1 - \cos \frac{\phi}{2} \cos \left(\theta + \frac{\phi}{2} \right) \right] \quad (5)$$

where d_p is the diameter of the piston.

For a single cycle, the ideal output fluid volume is then

$$V_{\text{idealout}} = \max(V) - \min(V) = \pi d_p^2 r \cos \frac{\phi}{2}. \quad (6)$$

With (6), the fractional displacement X of the AF pump can be obtained as follows:

$$X = \cos \frac{\phi}{2}. \quad (7)$$

The total effective displacement D per revolution of the AF pump is then

$$D = 2rnA_p X = \frac{\pi}{2} n d_p^2 r \cos \frac{\phi}{2} \quad (8)$$

where n is the number of pumping chambers (each with two pistons).

The change rates of cylinder volume of cylinder 1 and cylinder 2 from the same pair can be calculated by

$$\dot{V}_{\text{cyl},1} = A_p \omega r \left[1 + \frac{r \cos \theta}{\sqrt{l^2 - r^2 \sin^2 \theta}} \right] \quad (9)$$

$$\dot{V}_{\text{cyl},2} = A_p \omega r \left[1 + \frac{r \cos(\theta + \phi)}{\sqrt{l^2 - r^2 \sin^2(\theta + \phi)}} \right] \quad (10)$$

where ω is the pump rotating speed.

The bulk modulus is a fundamental property of a fluid that represents its compressibility. Entrained and dissolved air in hydraulic oil can significantly change the numerical value of the bulk modulus. Many researches have been done to establish the model of effective fluid bulk modulus though definitions are not consistent. A good collection and comparison of those models is presented in [17] and the effective bulk modulus β_{eff} in this work is calculated by

$$\beta_{\text{eff}} = \beta_0 \left[\frac{\left(\frac{P_{\text{cyl},i}}{P_o} \right)^{\frac{1}{\gamma}} e^{\frac{P_o - P_{\text{cyl},i}}{\beta}} + K}{\left(\frac{P_{\text{cyl},i}}{P_o} \right)^{\frac{1}{\gamma}} e^{\frac{P_o - P_{\text{cyl},i}}{\beta}} + \frac{K}{\gamma} \frac{\beta_0}{P_{\text{cyl},i}}} \right] \quad (11)$$

where β_0 is the bulk modulus of air free oil, P_o is the atmospheric pressure, γ is polytropic index for air/gas content, and K is entrained air fraction by volume.

A. Connecting Pipe Model

The two cylinders are directly connected with a pipe line, as shown in Fig. 1. A dynamic model for a short fluid pipeline with hydraulic resistance and inertance is established to calculate the flow rate Q_{con} . The fluid is assumed to be incompressible and inviscid in the connecting pipe line. This assumption is valid since the volume of the connecting pipe is small.

The pressure drop introduced by the connecting pipe hydraulic inertance I is calculated by

$$\Delta P_I = I \dot{Q}_{\text{con}} \quad (12)$$

$$I = \frac{\rho l_{\text{con}}}{A_{\text{con}}} \quad (13)$$

where \dot{Q}_{con} is the rate of change of flow rate in the connecting pipe, ρ is the oil density, l_{con} and A_{con} are the effective length and cross-sectional area of the connecting pipe, respectively.

The Reynolds number condition for a laminar flow in the connecting pipe is given by

$$Re_{\text{con}} = \frac{4\rho Q_{\text{con}}}{\pi \mu d_{\text{con}}} < 2300 \quad (14)$$

where Q_{con} is the flow rate in the connecting pipe, μ is the oil dynamic viscosity, and d_{con} is the diameter of the cross-sectional area of the connecting pipe.

The hydraulic resistance R and therefore, the pressure drop introduced by the connecting pipe resistance can be calculated

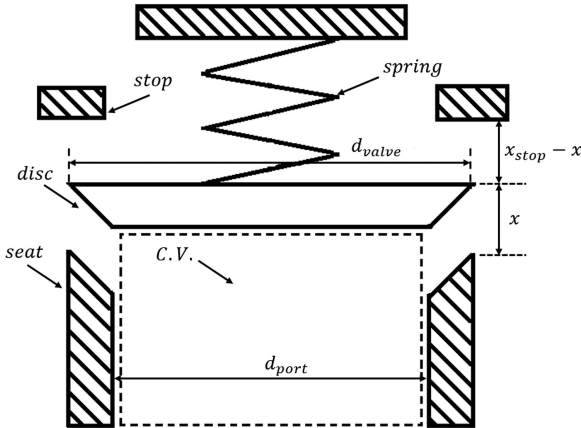


Fig. 3. Disc style check valve concept.

by

$$\Delta P_R = RQ_{\text{con}} \quad (15)$$

$$R = \frac{128\mu l_{\text{con}}}{\pi d_{\text{con}}^4}. \quad (16)$$

The dynamic equation for the flow rate between each pair of cylinders is

$$\dot{Q}_{\text{con}} = \frac{1}{I}(P_{\text{cyl},1} - P_{\text{cyl},2} - \Delta P_R). \quad (17)$$

B. Check Valve Model

A check valve is a passive flow control hydraulic device that ideally allows only unidirectional flow. The disc style check valve, shown in Fig. 3, utilizes a spring to seat a disc, which is of low mass and is able to respond quickly.

The dynamic motion equation for the disc is given by applying Newton's second law

$$m_{\text{disc}}\ddot{x} = F \quad (18)$$

where m_{disc} is the mass of the check valve disk, x is the position of the disc, and F is the summation of all external forces acting on the disc surface area A_{valve} . The main forces are hydraulic pressure force, F_{pressure} , spring force, F_{spring} , and seat/stop contact force, F_{contact} . Other external forces including stiction and flow force are negligible in general cases [18].

The pressure force F_{pressure} acting on the disc is introduced by the pressure difference across the check valve disc

$$F_{\text{pressure}} = \Delta P A_{\text{valve}}. \quad (19)$$

For the inlet check valve

$$\Delta P_{\text{in}} = P_{\text{tank}} - P_{\text{cyl},i}. \quad (20)$$

For the outlet check valve

$$\Delta P_{\text{out}} = P_{\text{cyl},i} - P_{\text{load}}. \quad (21)$$

The spring force F_{spring} is calculated by

$$F_{\text{spring}} = -k_{\text{spring}}(x + x_{\text{preload}}). \quad (22)$$

The allowable disc position is limited by the check valve seat ($x = 0$) and stop ($x = x_{\text{stop}}$). The contact force is modeled as the summation of elastic forces and dissipative reaction forces [18]

$$F_{\text{contact}} = \begin{cases} -k_{\text{seat}}x - C_{\text{seat}}\dot{x}, & \text{if } x < 0 \\ 0, & \text{if } 0 \leq x \leq x_{\text{stop}} \\ -k_{\text{stop}}(x - x_{\text{stop}}) - C_{\text{stop}}\dot{x}, & \text{if } x > x_{\text{stop}} \end{cases} \quad (23)$$

where the k_{seat} , C_{seat} , k_{stop} , and C_{stop} are check valve seat/stop spring stiffness and check valve seat/stop damping coefficient, respectively.

With (18) solved, the ring shape check valve orifice area $A_{\text{valve}}(x)$ can be expressed as a function of disc position x

$$A_{\text{valve}}(x) = \max(0, \pi d_{\text{port}}x). \quad (24)$$

The discharge coefficient of the check valve $C_{d\text{valve}}$ depends on check valve Reynolds number Re_{valve} . An empirical model is presented in [19] and a nonlinear least square experimental result is given in [18]

$$Re_{\text{valve}} = \frac{4\rho Q_{\text{valve}}}{\pi \mu d_{\text{port}}} \quad (25)$$

$$C_{d\text{valve}} = 0.79 - 0.87e^{-0.11\sqrt{Re_{\text{valve}}}} + 0.087e^{-0.95\sqrt{Re_{\text{valve}}}}. \quad (26)$$

With all necessary equations solved, the inlet flow rate from i th piston cylinder $Q_{\text{in},i}$ is

$$Q_{\text{in},i} = C_{d\text{valvein}} A_{\text{valvein}} \sqrt{\frac{2}{\rho} \Delta P_{\text{in}}}. \quad (27)$$

Similarly, the output flow rate from i th piston cylinder $Q_{\text{out},i}$ is

$$Q_{\text{out},i} = C_{d\text{valveout}} A_{\text{valveout}} \sqrt{\frac{2}{\rho} \Delta P_{\text{out}}}. \quad (28)$$

C. Load Model

A simple hydraulic circuit is set up for experimental tests, shown in Fig. 4. A nitrogen gas accumulator is precharged to regulate the downstream pressure P_{load} , which is adjusted by a variable orifice (VO) placed in parallel with a pressure relief valve. A bidirectional flow meter is placed downstream before the VO. The total output flow rate from the AF pump Q_{out} is the summation of all pairs of piston cylinders

$$Q_{\text{out}} = \sum Q_{\text{out},i}. \quad (29)$$

The flow rate relation is obtained by applying the law of mass conservation with the assumption of incompressible flow

$$Q_{\text{out}} = Q_{\text{acc}} + Q_{\text{vo}} \quad (30)$$

where Q_{acc} is the flow rate into the accumulator and Q_{vo} is the flow rate through the VO. A simple orifice model is used to model VO and its valve area A_{vo} is adjusted in such a way that

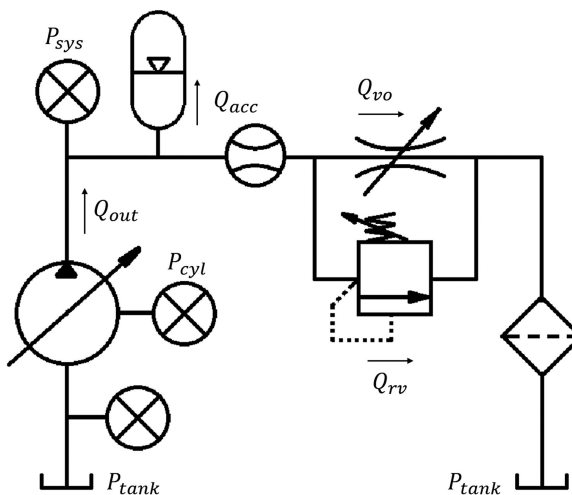


Fig. 4. Schematic of the experimental test setup.

the pressure is not high enough to open the pressure relief valve

$$Q_{vo} = C_d A_{vo} \sqrt{\frac{2}{\rho} (P_{load} - P_{tank})}. \quad (31)$$

The nitrogen gas in the accumulator is assumed to be adiabatic during compression and expansion, and the hydraulic fluid is assumed to be incompressible compared with nitrogen gas. Then, the load pressure P_{load} can be calculated by

$$\dot{V}_{acc} = -Q_{acc} \quad (32)$$

$$P_{load} = P_{charge} \left(\frac{V_{charge}}{V_{acc}} \right)^\gamma \quad (33)$$

where V_{charge} and V_{acc} are accumulator precharge gas volume and instantaneous accumulator gas volume.

IV. ENERGY MODEL

For the AF hydraulic pump, four types of energy losses are considered—leakage loss across the piston cylinder gap, viscous friction loss between piston and cylinder wall, check valve throttling loss, and connecting pipe resistance loss. The mechanical losses in the pump mechanism are neglected since this is not inherent to the concept. The motion of each piston is assumed to be only along the stroke direction, resulting in a constant gap height.

A. Leakage Loss Model

Leakage flow through the gap between the piston and the cylinder is created by a pressure drop across the piston. The leakage flow rate from the i th piston cylinder is given by [20]

$$Q_{leak,i} = \frac{\pi d_p h_p^3}{12 \mu l_p} (P_{cyl,i} - P_o) \quad (34)$$

where h_p is piston cylinder gap height and l_p is piston length.

Leakage energy loss from i th piston cylinder $E_{leak,i}$ can be obtained by integrating the product of leakage flow rate $Q_{leak,i}$

and cylinder pressure $P_{cyl,i}$ with respect to time

$$E_{leak,i} = \int (P_{cyl,i} - P_o) Q_{leak,i} dt. \quad (35)$$

B. Viscous Friction Loss Model

Viscous friction is introduced by shearing of the fluid between the piston and the cylinder. The viscous friction of i th piston cylinder is given by

$$F_{viscous,i} = \frac{\pi d_p l_p \mu}{h_p} \dot{y}_i \quad (36)$$

where \dot{y}_i is the velocity of the i th piston.

Viscous friction energy loss from i th piston cylinder $E_{viscous,i}$ can be obtained by integrating the product of viscous friction force $F_{viscous,i}$ and velocity of the i th piston \dot{y}_i with respect to time

$$E_{viscous,i} = \int F_{viscous,i} \dot{y}_i dt. \quad (37)$$

C. Check Valve Throttling Loss Model

Conventionally used check valves in hydraulic pumps inevitably introduce throttling losses. The instantaneous power of throttling for an inlet check valve is

$$\mathbb{P}_{throt,in,i} = \Delta P_{in} Q_{in,i}. \quad (38)$$

Similarly, the instantaneous power of throttling for an outlet check valve is

$$\mathbb{P}_{throt,out,i} = \Delta P_{out} Q_{out,i} \quad (39)$$

The throttling energy loss can then be calculated by integrating the instantaneous power with respect to time

$$E_{throt} = \int \mathbb{P}_{throt} dt. \quad (40)$$

D. Connecting Pipe Loss Model

Energy loss associated with connecting pipe E_{con} is calculated by integrating the product of the pressure difference across the connecting pipe resistance RQ_{con} and the flow rate through the connecting pipe Q_{con} with respect to time

$$E_{con} = \int RQ_{con}^2 dt. \quad (41)$$

E. Input Motor Torque Model

With the input crank angle θ known, the velocity and the acceleration of the i th piston can be calculated by

$$\dot{y}_i = r\dot{\theta} \sin \theta + \frac{r^2 \dot{\theta} \sin 2\theta}{2\sqrt{l^2 - r^2 \sin^2 \theta}} \quad (42)$$

$$\ddot{y}_i = r\dot{\theta}^2 \cos \theta + \frac{r^2 4\dot{\theta}^2 \cos 2\theta (l^2 - r^2 \sin^2 \theta) + r^2 \dot{\theta}^2 \sin^2 2\theta}{2(l^2 - r^2 \sin^2 \theta)^{3/2}} \quad (43)$$

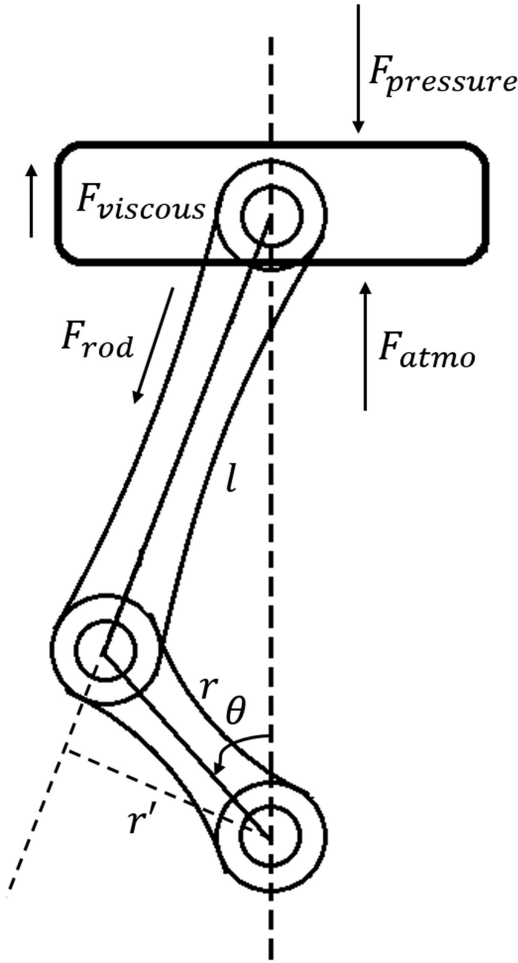


Fig. 5. Piston force diagram.

where a constant crank shaft speed assumption is made. This is a valid assumption for a high angular velocity and a crank shaft with sufficient inertia.

The dynamic motion equation for the piston is given by applying Newton's second law (as shown in Fig. 5).

$$m_{\text{piston}} \ddot{y}_i = F \quad (44)$$

where m_{piston} is the mass of the piston, F is the summation of all external forces. To simplify the model while maintaining accuracy, only cylinder pressure force $F_{\text{cyl},i}$, atmospheric force F_{atmo} , viscosity force $F_{\text{viscous},i}$, and rod force $F_{\text{rod},i}$ acting on the i th piston are considered.

The instantaneous hydraulic cylinder pressure force $F_{\text{pressure},i}$ acting on the i th piston is calculated by

$$F_{\text{pressure},i} = P_{\text{cyl},i} A_p. \quad (45)$$

The atmospheric pressure force F_{atmo} only acting on the other side of the i th piston is calculated by

$$F_{\text{atmo},i} = P_{\text{atmo}} A_p. \quad (46)$$

The viscous friction force $F_{\text{viscous},i}$ always acts along the opposite direction of the velocity of the i th piston. The rod force $F_{\text{rod},i}$ can therefore be calculated with (44) and the input

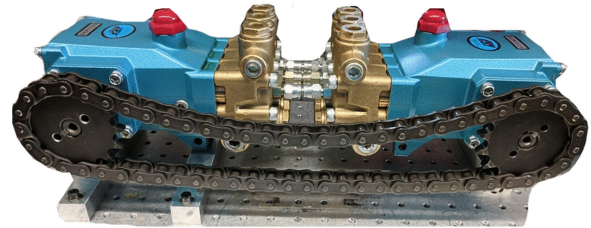


Fig. 6. Alternating flow pump prototype 1 created from two triplex piston pumps.

motor torque T_i to drive the i th piston can, therefore, be given by

$$T_i = F_{\text{rod}} r'_i. \quad (47)$$

The total input motor torque is, therefore, the summation of all T_i

$$T_{\text{motor}} = \sum T_i. \quad (48)$$

F. AF Pump Efficiency

All mechanical transmission torques T_{trans} are assumed to be constant and are out of the consideration of this design. The mechanical transmission work is calculated by

$$W_{\text{trans}} = \int \omega T_{\text{trans}} dt. \quad (49)$$

The total input work is calculated as

$$W_{\text{in}} = \int \omega T dt = \int \omega (T_{\text{motor}} + T_{\text{trans}}) dt. \quad (50)$$

The output fluid work is calculated as

$$W_{\text{out}} = \int Q_{\text{out}} P_{\text{load}} dt. \quad (51)$$

With input motor work and output fluid work determined, the total pump efficiency can be defined as

$$\eta_{\text{pump}} = \frac{W_{\text{out}}}{W_{\text{in}}}. \quad (52)$$

V. AF PUMP PROTOTYPE

To demonstrate the concept of the AF pump and validate the model developed previously, a prototype pump was designed, assembled, and tested. Instead of creating a complex device from scratch, a simplified version is preferred for the proof-of-concept prototype.

A. Methods

As shown in Fig. 6. Two 3CP1120 Cat Pump pumps were placed face to face with the crankshaft from one of them being reversed to synchronize the crankshaft rotation direction. Holes were drilled on top of each pair of cylinder chambers. A short hydraulic rigid pipe was used to connect each pair of cylinders. The cross-sectional view of this arrangement is shown in Fig. 7. To connect the two rotating crankshafts, a chain-and-sprocket transmission was used. To maintain tension on the chain, an

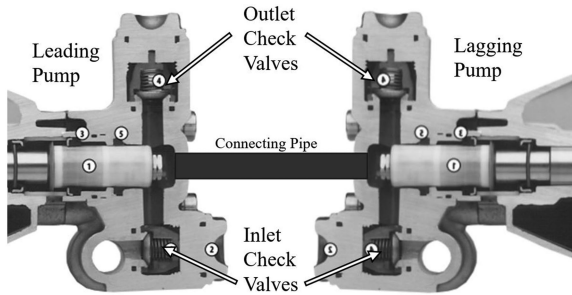


Fig. 7. Cross-sectional view of the two connected triplex piston pumps.

TABLE I
PROTOTYPE SPEC TABLE

Symbol	Description	Value
C_{seat}	Check valve seat damping coefficient	10^4 Ns/m
C_{stop}	Check valve stop damping coefficient	10^4 Ns/m
d_{con}	Connecting pipe diameter	4.2mm
d_p	Piston diameter	17.6mm
d_{port}	Check valve port diameter	8.2mm
d_{valve}	Check valve disk diameter	10.7mm
h_p	Piston cylinder gap height	9 μm
k_{seat}	Check valve seat spring stiffness	10^9 N/m
k_{stop}	Check valve stop spring stiffness	10^9 N/m
k_{spring}	Check valve spring stiffness	200N/m
l	Connecting rod length	43.81mm
l_{con}	Connecting pipe length	50mm
l_p	Piston length	10mm
m_{disc}	Mass of the check valve disc	5g
m_{piston}	Mass of the cylinder piston	50g
r	Crank radius	6.35mm
V_{tdc}	Cylinder top dead volume	7.95cm ³
$x_{preload}$	Check valve spring preload	6mm
x_{stop}	Maximum check valve displacement	3.52mm

adjustable idler gear is rigidly mounted halfway between the two pumps. The chain-and-sprocket allows for the measurement and adjustment of the phase angle between the pumps, although this requires disassembling the transmission. This disassembly requirement does not allow real-time adjustment of the phase which will be addressed in future prototypes. The detailed specifications of the prototype are given in Table I.

B. Experiment Setup

An experiment was devised to test the prototype pump and compare the simulated and measured efficiencies and dynamics. A schematic of the experiment system is shown in Fig. 4 and a diagram of the experiment showing the location of various sensors and hydraulic components is shown in Fig. 8. A nitrogen gas accumulator was precharged to regulate the downstream system pressure, which can be adjusted by a VO. A pressure relief valve was placed in parallel with the VO. The inlet pressure, the output pressure, and the pressure in the individual piston cylinder pairs were measured by Honeywell pressure transduc-

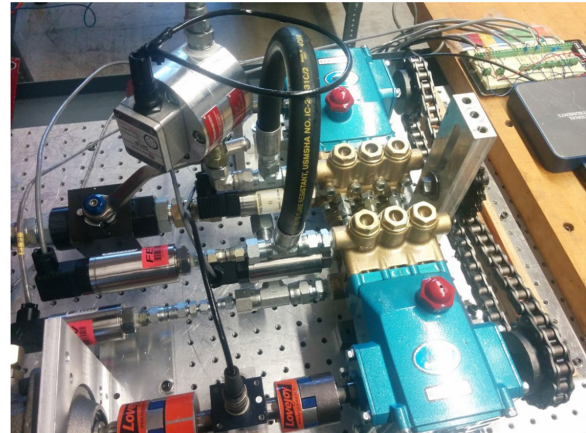


Fig. 8. First generation prototype of AF pump used for experiment validation.

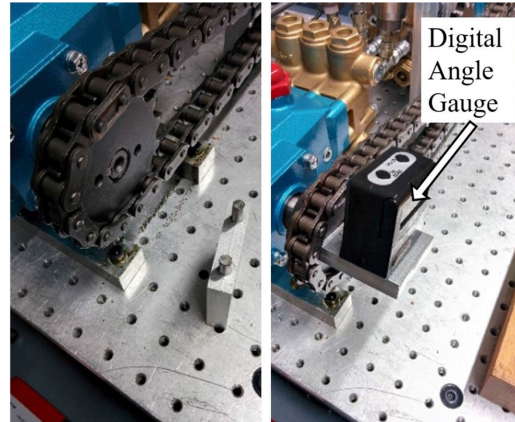


Fig. 9. Phase measuring fixture for AF pump.

ers. The two pressure transducers protruding from the side of the manifolds are to measure the pressure in each chamber of the piston pair and validate the pressure drop across the connecting pipe predicted by the model. The input motor torque was measured with a Futek TRS300 transducer and the rotary speed was measured with US Digital HB6M rotary encoder. An AW Lake gear flow meter measured the average output flow rate.

Experiments were run at a variety of phase-shift angles and speeds. The different phase angles were realized by disassembling the chain-and-sprocket transmission and rotating one of the sprockets on its associated crankshaft. The speed of the pump was managed by a hydraulic motor which was controlled by a flow control valve. To measure the crankshaft angle of each pump, a block with dowel pins was slid into a pair of the machined holes in the sprocket mounted to the crankshaft. The machined holes align with the keyway of the crankshaft at TDC of cylinder 1. A digital angle gauge was used to measure the angle of the leading crankshaft and the lagging crankshaft and the difference between the two was the phase shift. This fixture is shown in Fig. 9. The pressure, flow rate, torque, and optical encoder sensors were all read with a PCIe-6353 National Instruments DAQ board on a desktop computer. A series

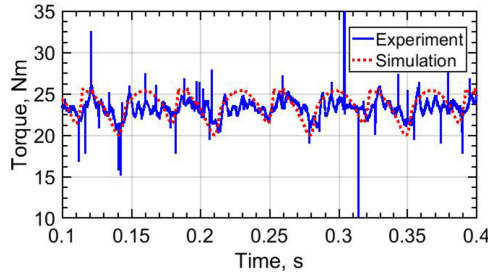


Fig. 10. Input motor torque comparison between experiment tests and model predictions at 2 degree phase-shift angle.

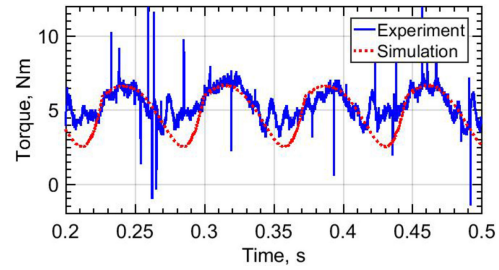


Fig. 11. Input motor torque comparison between experiment tests and model predictions at 165 degree phase-shift angle.

of experiments were run at all discrete phase angles achievable with the chain and sprocket. Once the transmission was installed and the phase angle was measured, the pump was driven by a hydraulic motor controlled with a flow control valve. For each experiment, the speed of the pump and load had to be set simultaneously due to the load being an adjustable orifice. Once the speed and pressure were set, the DAQ acquired data for three seconds after the system reaches a steady state at a rate of 10 Ks/s.

The measured system pressure, flow rate, input torque, and shaft speed are used to calculate the total efficiency of the pump, given as

$$\eta_{\text{pump}} = \eta_m \eta_v \quad (53)$$

$$\eta_m = \frac{P_{\text{load}} D}{2\pi T} \quad (54)$$

$$\eta_v = \frac{2\pi Q_{\text{out}}}{\omega D} \quad (55)$$

where η_m is the mechanical efficiency and η_v is the volumetric efficiency.

VI. MODEL VALIDATION

A series of experiments were conducted with various operating conditions and displacements. The crankshaft speed varied from 4.167 Hz (250 r/min) to 16.667 Hz (1000 r/min) while the system pressure was held constant at 6.895 MPa (1000 psi). The achievable phase shift angles were determined by the number of teeth of the sprockets. The minimum available phase angle was 2 degrees and the maximum was 165 degrees.

Two different torque versus time curves are shown in Figs. 10 and 11 under the operating condition of 4.167 Hz (250 r/min) and 6.895 MPa (1000 psi), with phase-shift angle of 2 degrees and 165 degrees, respectively. The dynamic model for the input torque correlates well with the experimental results. As can be shown from the comparison between Figs. 10 and 11, the motor driving torque required reduces as the phase-shift angle increases. This can be explained by the motoring effect introduced by the connecting pipe mechanism.

Two different pressure versus volume curves are shown in Figs. 12 and 13, both showing a full cycle of the AF pump operating at 4.167 Hz (250 r/min) and 6.895 MPa (1000 psi), with phase-shift angle of 2 degrees and 165 degrees, respectively.

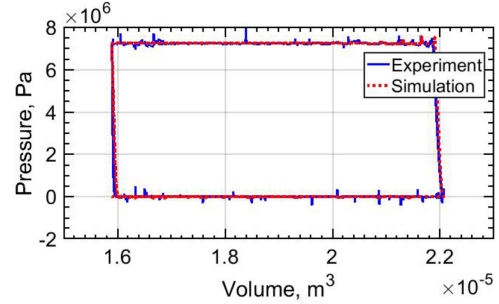


Fig. 12. PV curve comparison between experiment tests and model predictions at 2 degree phase-shift angle.

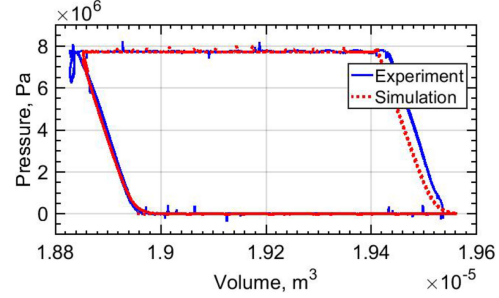


Fig. 13. PV curve comparison between experiment tests and model predictions at 165 degree phase-shift angle.

The model agrees well with the pressure versus volume plots except for the 165 degree case once the pressure in the chamber starts to decrease, as shown in the top-left portion of Fig. 13. Some insight into what may be happening at this point in the cycle can be seen in Fig. 14, where about halfway through the compressed volume cycle there is a dip in pressure of 1 MPa (145 psi). The numerical model was not able to capture this effect well, which is evident in the pressure versus volume curves, but does not affect the measured and modeled energy curves. This is likely due to the piston motion not being perfectly sinusoidal due to the kinematics of the crank slider, a slight negative change in the total volume of the two cylinders at the high phase-shift angle.

Fig. 15 compares the input motor torque work done in 0.5 seconds from the experimental measures and from the previously described model. Fig. 16 shows the output fluid energy in 0.5 seconds from experimental measures and from the model. As

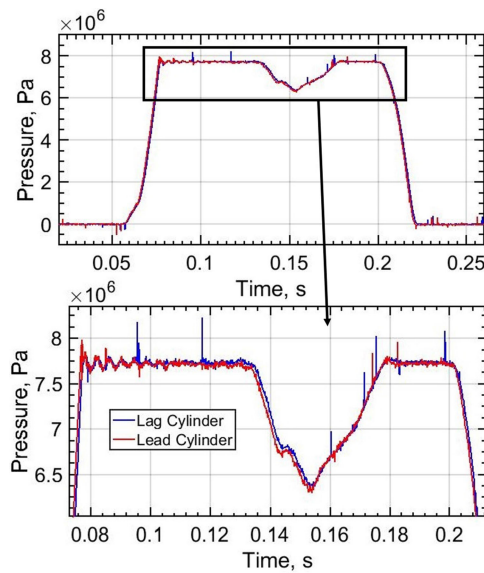


Fig. 14. Pressure signal at either end of connecting pipe for 165 degree phase-shift angle.

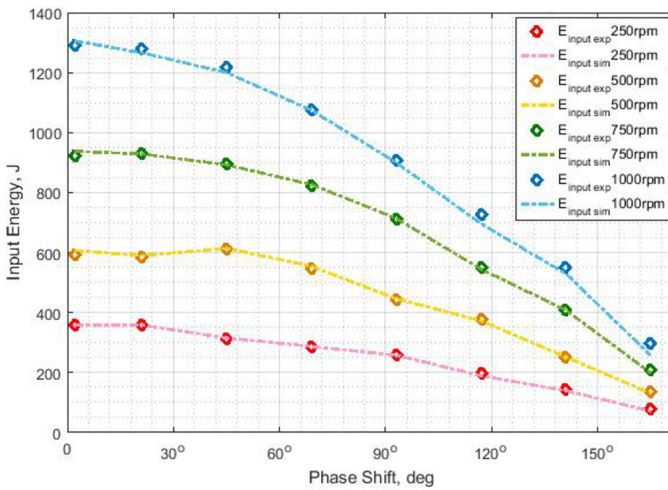


Fig. 15. Input energy comparison between experiment tests and model predictions.

can be seen from Figs. 15 and 16, the model shows close agreement to the experiment results for both input and output energy. The reason behind the unevenness of the efficiency curves is that for each conducted test, the shaft speed and the system pressure varied around the nominal values due to the coarse control of the experimental setup.

The input model matches with experimental data closer than the output model does for all operating conditions and displacements. This is mainly because the input model depends on the experimental system pressure and crankshaft speed data. The output model is capable of matching with experimental data for most of the operating conditions and displacements while the discrepancies become bigger as the phase-shift angle becomes higher. Many things can cause this phenomenon. First of all, the inaccuracy of the simple crank slider motion model

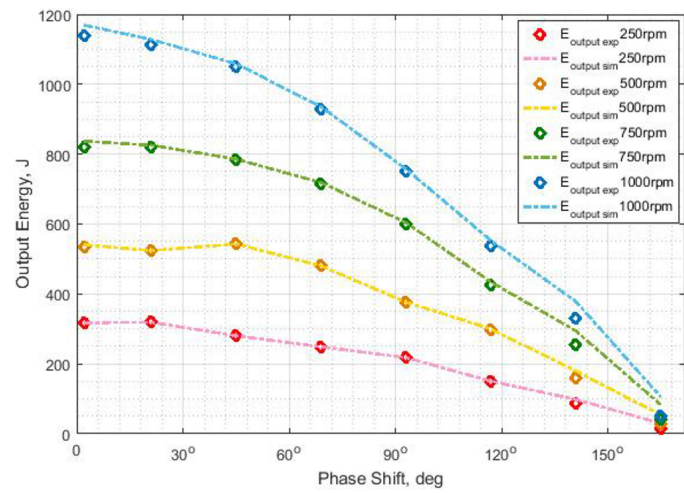


Fig. 16. Output energy comparison between experiment tests and model predictions.

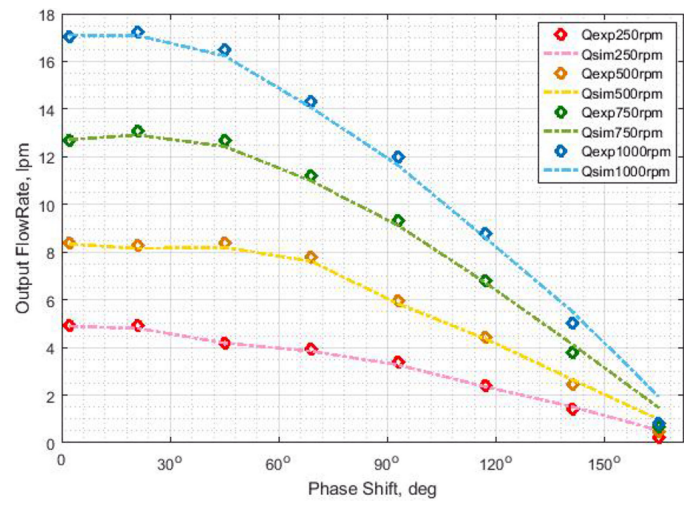


Fig. 17. Output flow rate comparison between experiment tests and model predictions.

increases as the phase-shift angle approaches 180 degrees. The model predicted output flow rate then diverges from the experimental data, which is shown in Fig. 17. Second, for simplicity, two inline triplex water pumps with bigger unswept dead volume, compared with normal hydraulic pumps, were chosen to build the prototype. As the displaced volume compared with the cylinder volume is quite small at the high phase angle, the inaccuracies in the predicted fluid effective bulk modulus become magnified. Third, at high phase angle, the actual geometry structure of the connecting pipe introduces complicated dynamics and a more complex model is needed to accurately describe it.

VII. DISCUSSION

With the dynamic model validated, it can be used to explore the parameter space and guide design optimization of future generation prototypes.

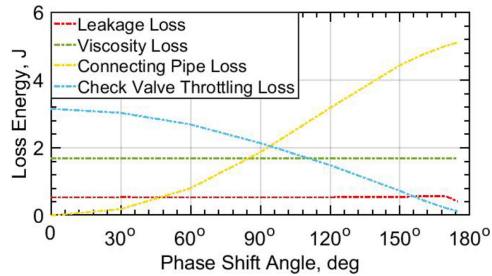


Fig. 18. Four types of energy loss versus phase-shift angle.

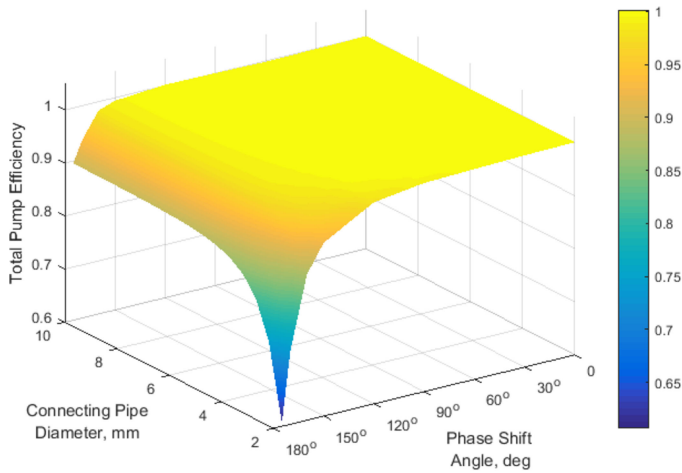


Fig. 19. Model predicted efficiency versus phase-shift angle and connecting pipe diameter.

Although the connecting pipe offers a mechanism for two piston cylinders to balance their pressure levels, some energy is dissipated in the form of hydraulic resistance. Fig. 18 plots the four modeled energy losses accumulated in 0.5 seconds versus different phase-shift angles. It can be seen that the hydraulic resistance loss introduced by the connecting pipe is a function of the phase-shift angle ϕ . Also note that the check valve throttling loss drops as the phase-shift angle increases. These phenomena agree with the basic principles of the AF hydraulic pump since more fluid is shuttled through the connecting pipe at higher phase-shift angles.

Many different types of mechanical losses exist in the transmission parts of every hydraulic pump and a huge chain-and-sprocket was used in this first generation prototype AF pump. Therefore, those mechanical transmission losses are not in the scope of design consideration and are neglected here.

To optimize the connecting pipe structure of the AF hydraulic pump, the model predicted pump efficiency is plotted in Fig. 19 against various phase-shift angles and different connecting pipe diameters ranging between 2 and 10 mm with a constant connecting pipe length of 50 mm. Fig. 20 plots the model predicted pump efficiency versus various phase-shift angles and different connecting pipe lengths ranging from 10 to 150 mm with a constant connecting pipe diameter of 4.2 mm under the same operating pressure and frequency conditions. Generally, it can be seen that the AF hydraulic pump prefers a short and large

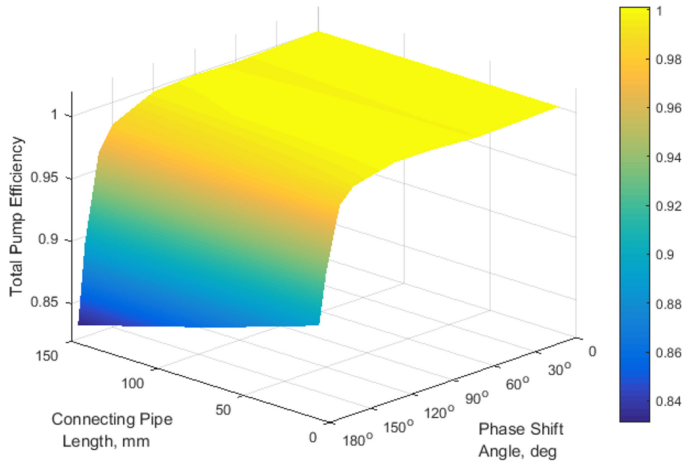


Fig. 20. Model predicted efficiency versus phase-shift angle and connecting pipe length.

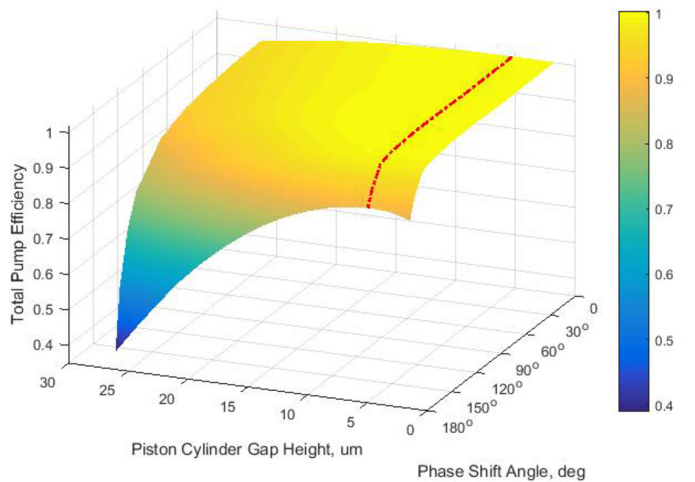


Fig. 21. Model predicted efficiency versus phase-shift angle and piston cylinder gap height.

connecting pipe to minimize the energy loss associated with hydraulic pipe resistance. Once the diameter of the connecting pipe reaches approximately 4 mm, for the first-generation prototype, the overall pump efficiency remains high across most of the phase-shift angles. The AF pump favors a short connecting pipe to: 1) reduce the associated energy loss and 2) avoid complicated phenomena brought by long hydraulic pipes such as reflected pressure waves.

The predicted pump efficiency curve against various phase-shift angles and piston cylinder gap heights varying between 1 and 28 μm under the same operating conditions, is shown in Fig. 21. It shows that the optimal piston cylinder gap height (red dash line) is independent of the different phase-shift angles ϕ . This result shows an agreement with minimum energy dissipation analysis [21] and with the closed form model developed by Li et al. [22]. Unlike the connecting pipe, due to manufacturing inaccuracy, the piston cylinder gap height cannot be made small.

With all mechanical losses of the AF pump mechanism taken out of design consideration, a series of simulations were run

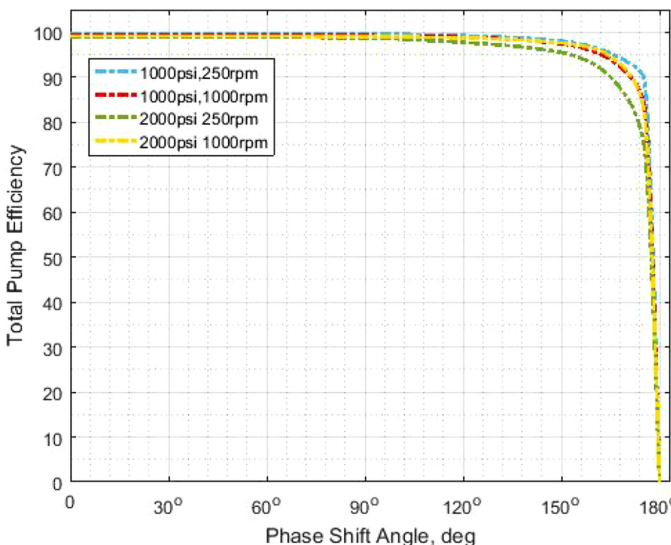


Fig. 22. Model predicted efficiency versus phase-shift angles.

with various operating conditions and displacements. The load pressure varied between 6.895 (1000) to 13.789 MPa (2000 psi) and the input shaft speed were between 4.167 (250) to 16.667 Hz (1000 r/min). The phase-shift angles varied between 0 and 175 degrees and is shown in Fig. 22.

VIII. CONCLUSION

This paper presents the basic principles and advantages of a novel AF hydraulic pump. A dynamic model describing the cylinder pressure, the flow between a pair of cylinders, and the inlet and output flow as a function of phase-shift angle is developed in detail. The hydraulic check valve dynamics and the effective bulk modulus are taken into consideration. A first-generation prototype was built with two inline triplex Cat Pump pumps to demonstrate the concept. Experiments were run and data was collected to validate the model. With the model validated, it can be used to explore the parameter space and optimize future prototype designs. Taking four types of energy losses into consideration, the model results show that the novel AF hydraulic pump is able to achieve high efficiencies of greater than 90% for displacements greater than 10% (approximately 168 degrees phase shift).

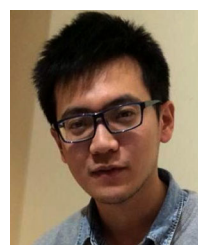
ACKNOWLEDGMENT

The authors would like to thank Cat Pump for donating the experimental prototype.

REFERENCES

- [1] L. J. Love, "Estimating the impact (energy, emissions and economics) of the U.S. fluid power industry," Oak Ridge Nat. Lab., Oak Ridge, TN, USA, Tech. Rep. ORNL/TM-2011/14, 2012.
- [2] K. Heybroek, "Saving energy in construction machinery using displacement control hydraulics: Concept realization and validation," Ph.D. dissertation, Linköping University, Linköping, Sweden, 2008.

- [3] C. Williamson, "Efficiency study of an excavator hydraulic system based on displacement-controlled actuators," in *Proc. Bath/ASME Symp. Fluid Power Motion Control*, 2008, pp. 291–307.
- [4] M. Ivantysynova, "Innovations in pump design—What are future directions?" in *Proc. IFPS Int. Symp. Fluid Power*, 2008, vol. 2008, pp. 59–64.
- [5] C. Zhang, S. Huang, J. Du, X. Wang, S. Wang, and H. Zhang, "A new dynamic seven-stage model for thickness prediction of the film between valve plate and cylinder block in axial piston pumps," *Adv. Mech. Eng.*, vol. 8, no. 9, pp. 1–15, 2016.
- [6] L. Shang and M. Ivantysynova, "A temperature adaptive piston design for swash plate type axial piston machines," *Int. J. Fluid Power*, vol. 18, no. 1, pp. 38–48, 2017.
- [7] G. Rizzo *et al.*, "Axial piston pumps slippers with nanocoated surfaces to reduce friction," *Int. J. Fluid Power*, vol. 16, no. 1, pp. 1–10, 2015.
- [8] S. R. Wilhelm and J. D. Van de Ven, "Synthesis of a variable displacement linkage for a hydraulic transformer," in *Proc. ASME Int. Des. Eng. Tech. Conf. Comput. Inf. Eng. Conf.*, 2011, pp. 309–316.
- [9] S. Wilhelm and J. Van de Ven, "Adjustable linkage pump: Efficiency modeling and experimental validation," *J. Mechanisms Robot.*, vol. 7, no. 3, 2015, Art. no. 031013.
- [10] S. Wilhelm and J. D. Van de Ven, "Design of a variable displacement triplex pump," in *Proc. Int. Fluid Power Expo.*, Las Vegas, NV, USA, 2014, pp. 1–8.
- [11] M. Ehsan, W. Rampen, and S. Salter, "Modeling of digital-displacement pump-motors and their application as hydraulic drives for nonuniform loads," *J. Dyn. Syst., Meas., Control*, vol. 122, no. 1, pp. 210–215, 2000.
- [12] M. Linjama, "Digital fluid power: State of the art," in *Proc. 12th Scand. Int. Conf. Fluid Power*, Tampere, Finland, May 2011, pp. 18–20.
- [13] G. Constantinesco, *Theory of Wave Transmission: A Treatise on Transmission of Power by Vibrations*, vol. 1, London, U.K.: W. Haddon, 1922.
- [14] C.-K. Weng, "Transmission of fluid power by pulsating-flow (PF) concept in hydraulic systems," *J. Basic Eng.*, vol. 88, no. 2, pp. 316–321, 1966.
- [15] D. C. Davis, "On alternating flow hydraulic systems," Ph.D. dissertation, Monash Univ., Melbourne, Australia, 1982.
- [16] I.-L. Marcu, "A new concept of rotary hydraulic motor working with alternating flows," *Trans. Mech.*, vol. 49, no. 63, pp. 361–362, 2004.
- [17] H. Gholizadeh, R. Burton, and G. Schoenau, "Fluid bulk modulus: Comparison of low pressure models," *Int. J. Fluid Power*, vol. 13, no. 1, pp. 7–16, 2012.
- [18] A. L. Knutson and J. D. Van de Ven, "Modelling and experimental validation of the displacement of a check valve in hydraulic piston pump," *Int. J. Fluid Power*, vol. 17, no. 2, pp. 114–124, 2016.
- [19] D. Wu, R. Burton, and G. Schoenau, "An empirical discharge coefficient model for orifice flow," *Int. J. Fluid Power*, vol. 3, no. 3, pp. 13–19, 2002.
- [20] J. S. Cundiff, *Fluid Power Circuits and Controls: Fundamentals and Applications*. Boca Raton, FL, USA: CRC Press, 2001.
- [21] J. Ivantysyn and M. Ivantysynova, *Hydrostatic Pumps and Motors: Principles, Design, Performance, Modelling, Analysis, Control and Testing*. Falls Church, VA, USA: Tech Books International, 2003.
- [22] M. Li, R. Foss, K. A. Stelson, J. D. Van de Ven, and E. J. Barth, "A design optimization model for an alternating flow (AF) hydraulic pump based on first principles," in *Proc. ASME Dyn. Syst. Control Conf.*, 2017, Paper DSAC2017-5171.



Mengtang Li received the B.S. degree with honor in astronautics engineering from Northwestern Polytechnical University, Xi'an, China, and the M.S. degree in electrical engineering from Vanderbilt University, Nashville, TN, USA, in 2014 and 2016, respectively. He is currently working toward the Ph.D. degree in mechanical engineering at Vanderbilt University.

His research interests include compact and efficient fluid power, hydraulic pump/motor design, and mechanical circulatory support device design and optimization.



Ryan Foss received the B.S. degree in mechanical engineering in 2016 from the University of Minnesota, Minneapolis, MN, USA, where he is currently working toward the M.S. degree in mechanical engineering.

He is currently a Software Engineer with the Toro Company, Bloomington, MN, USA. His current research interest involves the design and testing of a novel variable displacement hydraulic pump and modeling and testing a frequency addressable hydraulic valve.



James D. Van de Ven received the Ph.D. degree in mechanical engineering from the University of Minnesota, Minneapolis, MN, USA, in 2006. He was a Postdoctoral Research Associate with the University of Minnesota in the NSF sponsored Engineering Research Center for Compact and Efficient Fluid Power.

From 2007 to 2011, he was an Assistant Professor with the Mechanical Engineering Department at Worcester Polytechnic Institute. He is currently an Associate Professor with the Department of Mechanical Engineering, University of Minnesota, where he operates the Mechanical Energy and Power Systems (MEPS) Laboratory. His research interests are in efficient energy conversion, energy storage, fluid power, kinematics, and machine design.



Kim A. Stelson received the B.S. degree from Stanford University, Palo Alto, CA, USA, in 1974, and the S.M. and Sc.D. degrees from the Massachusetts Institute of Technology, Cambridge, MA, USA, in 1977 and 1982.

Since 1981, he has been with the University of Minnesota, Minneapolis, MN, USA. He is currently a CSE Distinguished Professor and founding Director of the National Science Foundation Engineering Research Center for Compact and Efficient Fluid Power. His research interests include system dynamics, control, manufacturing, and fluid power.

Prof. Stelson is a recipient of the ASME Koski Medal and a Fellow of ASME and AAAS.



Eric J. Barth received the B.S. degree in engineering physics from the University of California at Berkeley, Berkeley, CA, USA, and the M.S. and Ph.D. degrees in mechanical engineering from the Georgia Institute of Technology, Atlanta, GA, USA, in 1994, 1996, and 2000, respectively.

He is currently an Associate Professor of Mechanical Engineering with Vanderbilt University, Nashville, TN, USA. His research interests include the design, modeling and control of mechatronic and fluid power systems, free-piston internal combustion and free-piston Stirling engines, energy storage and energy harvesting, MRI compatible pneumatic robots, and applied nonlinear control.